PHYSICAL REVIEW B **80**, 161202(R) (2009)

Unusual domain-wall motion in ferromagnetic semiconductor films with tetragonal anisotropy

C. Gourdon,[1] V. Jeudy,[1,2] A. Cēbers,[3] A. Dourlat,[1] Kh. Khazen,[1] and A. Lemaître[4]
[1]*Institut des Nanosciences de Paris, UPMC, CNRS UMR 7588, 140 rue de Lourmel, Paris F-75015, France*
[2]*Université de Cergy-Pontoise, 95000 Cergy-Pontoise, France*
[3]*Institute of Physics, University of Latvia, Salaspils-1 LV-2169, Latvia*
[4]*Laboratoire de Photonique et Nanostructures, CNRS, UPR 20 Route de Nozay, Marcoussis F-91460, France*
(Received 8 September 2009; published 13 October 2009)

Magnetic field-driven domain-wall propagation in the flow regime is investigated in (Ga,Mn)As ferromagnetic semiconductor layers. Square-shape magnetic domains with an unexpected orientation of their edges, at $\pi/8$ with respect to the anisotropy axes, are found. This is shown to arise from the effect of tetragonal magnetic anisotropy on domain-wall dynamics. Using a one-dimensional model for domain-wall motion and modeling domain growth by contour dynamics the shape and orientation of domains and their field range for existence are well reproduced. These results point to the key role of the vectorial nature of the order parameter in the dynamics of ferromagnetic domains.

DOI: 10.1103/PhysRevB.80.161202 PACS number(s): 75.30.Gw, 75.50.Pp, 75.60.Jk, 75.70.Kw

Anisotropy plays an important role in the formation of complex phase boundaries in dynamical processes of phase transitions, as for example crystal growth from the liquid phase in directional solidification experiments,[1–3] or in multiphase fluid flow in a Hele-Shaw cell.[3,4] In particular the role of surface-tension anisotropy in the selection of the fingering or dendritic patterns was recognized. Anisotropy is also intimately related to the formation of quasiequilibrium domain structures for various two-dimensional physical systems: submonolayer of adsorbed atoms on a metal substrate,[5] Si(111) surface near a structural phase transition,[6] intermediate state of type-I superconductor films,[7] ferrimagnetic garnets[8–12] and ultrathin ferromagnetic films.[13,14] Anisotropy of the interface energy or of the diffusion coefficient results in an alignment of lamellar domains[5,7] along specific crystallographic directions, and produces triangular[6,13] or square[5] domain shapes instead of the circular ones observed in the isotropic case.

In ferri- and ferromagnetic systems, the growth of a magnetic domain by propagation of a magnetic domain wall (DW) is rather singular due to the vectorial nature of the order parameter. Magnetic field-driven DW dynamics was extensively studied in films with out-of-plane easy axis.[15–18] Different dynamical flow regimes are expected to occur, depending on the field strength and on the DW structure. At low drive, the DW structure is steady (steady regime) and the DW differential mobility (field derivative of the velocity) is constant up to the so-called Walker limit. Above this limit the magnetization within the wall precesses around the applied field (precessional regime). The DW oscillates back and forth during its motion, which leads to a negative average differential mobility. The wall structure might become unstable with the generation of Bloch lines[16] or wall-displacement waves.[19] At high drive, the DW recovers a positive and constant differential mobility. The first evidences for anisotropic DW motion were found in orthoferrites[8,20] and in garnet films grown under strong compression.[9–11] These materials present an orthorhombic anisotropy: in addition to an out-of-plane easy axis, the films have a secondary in-plane easy axis. This produces static domains elongated in the direction of the in-plane easy axis[21] and dynamic elongation of domains in the perpendicular direction.[9] This phenomenon is usually explained as a result of an anisotropic mobility in orthoferrites[8] or of an anisotropic Walker velocity limit in garnets.[11] However, for garnets, the experimental maximum velocity[11] is found in many cases in poor agreement with the theoretical predictions,[21] which suggests that the contribution of anisotropy to the dynamics of magnetization reversal in not well understood. Furthermore the conditions for existence of an anisotropic DW motion (field range, temperature) have not been investigated. Therefore, it is particularly interesting to study a system presenting a different symmetry as an in-plane biaxial symmetry (tetragonal anisotropy). This is also expected to provide new insights into the specificity of interface propagation in ferromagnetic materials compared to other physical systems.

Diluted ferromagnetic semiconductors such as (Ga,Mn)As are appropriate materials for this purpose. Owing to the carrier-mediated ferromagnetism between the Mn ions, the magnetic anisotropy is mainly band engineered because of the very low saturation magnetization of (Ga,Mn)As, and the quenching of the Mn orbital moment (for a review see, e.g., Ref. 22). Band engineering via strain control in epitaxial layers provides a mean to obtain a perpendicular-to-plane easy axis.[23] The respective contributions of the weak uniaxial and biaxial in-plane anisotropies can be tuned by temperature.[24] Moreover, our recent results on field-driven DW propagation show that, owing to a depinning field much smaller than in ferromagnetic ultrathin metallic layers, not only the precessional flow regime but also the end of the steady flow regime can be observed.[18] In that first study devoted to the determination of micromagnetic parameters from these two dynamical regimes domain anisotropy, although observable in some range of field and temperature, was not analyzed.

In this Rapid Communication we concentrate on the formation of square magnetic domains in ferromagnetic (Ga,Mn)As. The edges of the domains are found to be oriented at $\pi/8$ of the in-plane secondary easy axes. We show that this shape and orientation originate from the effect of the tetragonal anisotropy of the sample on DW dynamics.

The sample consists of an annealed $Ga_{0.93}Mn_{0.07}As$ epil-

ayer of thickness $d=50$ nm grown on a relaxed $Ga_{0.902}In_{0.098}As$ buffer deposited on a GaAs substrate. The Curie temperature T_C is 130 K and the magnetic easy axis is perpendicular to the sample plane. The magnetization $M(T)$ was obtained from magnetometry measurement and the anisotropy constants from ferromagnetic resonance (FMR) experiments.[25] In the temperature range of interest ≈80 to 110 K, the perpendicular magnetic anisotropy constant K_u is 10–80 times larger than the in-plane biaxial anisotropy constant $K_{4\|}$ (difference between the ⟨100⟩ axes and the ⟨110⟩ axes) and more than 20 times larger than the in-plane uniaxial constant $K_{2\|}$ (difference between the [110] and $[1\bar{1}0]$ axes). Interestingly, $K_{2\|}$ vanishes around T=100 K so that the sample presents a pure tetragonal anisotropy. Kerr microscopy is used for the observation of DW motion (see Refs. 23 and 26 for more details). The DW velocity is measured using a magnetic pulse field technique.[17,18] The DW width Δ and the damping coefficient α are obtained from the analysis of the experimental velocity curve.[18]

Figures 1(a)–1(c) show the magnetic domain expansion and domain shapes for increasing values of the applied magnetic field. These differential images result from the substraction of an image taken before the application of a field pulse from the image taken after the pulse. The white corona represents the displacement of the DW as observed after the pulse. The black holes at the center correspond to domain areas before the pulse. In Fig. 1(a) irregular interfaces are seen. They result from DW pinning by defects.[23,26] In Figs. 1(b) and 1(c) smooth interfaces show that DWs move in the defect-independent flow regime. It is clearly seen in Figs. 1(a) and 1(b) that the magnetic domains exhibit a square shape. This square shape has almost disappeared at higher field [Fig. 1(c)]. Square domains have a fixed orientation. Surprisingly their edges are aligned neither along the ⟨100⟩ in-plane easy axes nor along the ⟨110⟩ in-plane hard axes but at 19 ± 5 degrees of a ⟨110⟩ axis, i.e., nearly at $\pi/8$. Moreover, when the direction of magnetization inside the domains is reversed the orientation of the square domains is rotated by $\approx\pi/4$, i.e., toward a symmetrical position with respect to a ⟨110⟩ axis, as displayed in Fig. 1(d). This indicates that the domain orientation is not controlled by pinning defects. The fourfold symmetry of the domain shape suggests a contribution of the in-plane biaxial magnetic anisotropy.

In order to investigate the field dependence of domain anisotropy, the DW velocity was measured along the diagonal of the square domains and perpendicularly to their edges, as shown by arrows on the inset of Fig. 1(e). The measured values are reported as a function of the applied field in Fig. 1(e). The velocity along the diagonal is at most 15% larger than the edge velocity. DW anisotropy is observed in the field range from ≈5 to 25 mT. The lower limit is close to the end of the steady regime, as determined from the Walker field ($\mu_0 H_W=\alpha\mu_0 M/2=4$ mT).[18] This suggests that the appearance of this anisotropy is related to the onset of the magnetization precession around the applied field inside the DW.

In order to obtain a more quantitative insight into anisotropic DW motion we use the standard one-dimensional (1D) model.[15,16] Indeed, this model has been successfully used to describe the steady regime and the high-field linear precessional regime in (Ga,Mn)As layers.[18] We introduce the in-plane biaxial magnetic anisotropy, which up to now has not been taken into account. In this framework the DW is modeled as an infinite plane wall with a homogeneous magnetic structure within the film thickness. The DW is assumed to lie in the xz plane, the DW velocity being along the y direction. The magnetic field H_0 is applied along z. The magnetization vector inside the DW is described by the polar angle θ and the azimuthal angle φ. The DW surface energy σ is defined as $\sigma=\int e dy$, where $e=e_0+e_1$ is constructed as

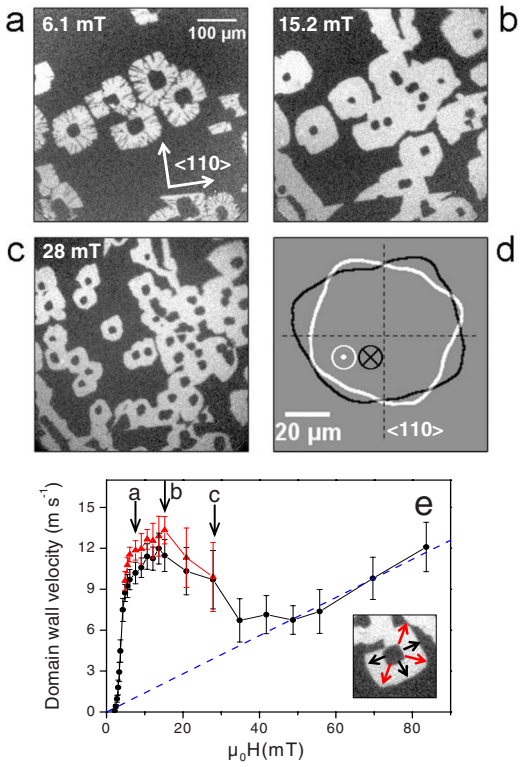

FIG. 1. (Color online) Magneto-optical images showing the square domains at T=100 K for three field values shown by arrows in (e). Images (a)–(c) are differential images (see text). Image (d): square domain edge with up (white) or down (black) magnetization inside the domain showing the $+\pi/8$ or $-\pi/8$ orientation of the diagonal of the square domain with respect to a ⟨110⟩ axis (dotted black lines). (e) DW velocity curve at $T=100$ K. In the field range where square domains are observed the red triangles and the black circles represent the velocity measured along the diagonal and perpendicularly to the edges of the domains, respectively, as shown in the inset. The error bars represents the width of the velocity distribution measured for a set of domains over a (536 μm)^2 area. The dashed line represents the asymptotic linear fit of the high-field precessional regime.

$$e_0 = A(\theta'^2 + \sin^2\theta\varphi'^2) + K_u \sin^2\theta, \tag{1}$$

$$e_1 = (\mu_0/2)M^2 \sin^2\theta \sin^2\varphi - K_{4\|} \sin^4\theta \sin^2[2(\varphi+\varphi_p)] - \mu_0 M H_0 \cos\theta. \tag{2}$$

The term e_0 contains the exchange energy (exchange constant A) and the uniaxial magnetic anisotropy energy. The term e_1 contains the DW demagnetizing energy, the in-plane

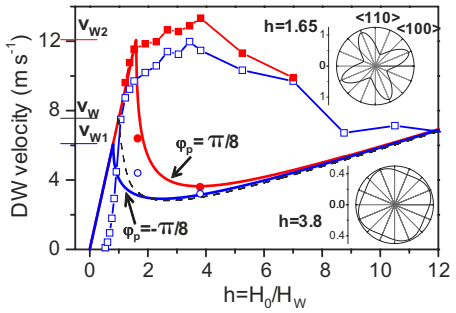

FIG. 2. (Color online) Experimental (squares) and theoretical (full curves) DW velocity curves at $T=100$ K. In the field range where square domains are observed the red full squares and the blue empty squares represent the velocity measured along the diagonal and perpendicularly to the edges of the domains, respectively. The red (blue) full line is the normal velocity calculated for $\varphi_p=\pi/8$ $(-\pi/8)$ orientation of the DW. The full (empty) circles show the maximum (minimum) velocity obtained from contour dynamics for two field values $h=1.65$ and $h=3.8$. The dashed black line is the velocity obtained when neglecting the in-plane magnetic anisotropy. The Walker velocities without anisotropy (v_W) and with biaxial anisotropy (v_{W1} and v_{W2}) are indicated. The parameters are $H_W=4$ mT, $\Delta=3$ nm, $\alpha=0.28$, and $\chi_4=0.6$. The insets show the angular dependence of the normal velocity (in units of v_W).

biaxial magnetic anisotropy energy and the Zeeman energy. φ_p is the angle between the normal to the DW and the [110] axis. The prime denotes the y-derivative. Note that for the static case σ is minimum for DWs aligned along the in-plane easy axes. The equations for DW motion are derived from the Landau-Lifshitz equations integrated through the wall thickness.[15,16] Treating the e_1-part of the DW energy in perturbation theory, we obtain

$$v = v_W h - \frac{\Delta\dot{\varphi}}{\alpha}, \tag{3}$$

$$\dot{\varphi} = \frac{\gamma H_W}{1+\alpha^2}\{h - [\sin(2\varphi) - \chi_4 \sin(4(\varphi+\varphi_p))]\}, \tag{4}$$

where v is the DW normal velocity, γ the gyromagnetic factor ($\gamma>0$), $v_W=\gamma\Delta\mu_0 M/2$ the Walker velocity, $H_W=\alpha M/2$ the Walker field, and $h=H_0/H_W$. $\chi_4=(4/3)K_{4\|}/(\mu_0 M^2/2)$ is positive ($\langle 100\rangle$ in-plane easy axes). In the steady regime ($\dot{\varphi}=0$) the DW velocity varies linearly with the field: $v=v_W h$. In the precessional regime ($\dot{\varphi}\neq 0$) one defines an average velocity as

$$\langle v\rangle = v_W\left(h - \frac{\pi}{\gamma H_W T}\right), \tag{5}$$

$$\frac{\gamma H_W T}{(1+\alpha^2)} = \int_0^{\pi} \frac{d\varphi}{h - [\sin(2\varphi) - \chi_4 \sin(4(\varphi+\varphi_p))]}, \tag{6}$$

where T is the period of the magnetization precession. Equation (5) shows that the precession reduces the DW velocity. Moreover, one finds from Eqs. (3) and (4) that the value of the magnetic field separating the steady and the precessional regimes depends on the DW orientation φ_p. Therefore, the DW velocity can be anisotropic due to the anisotropic term $\sin(4(\varphi+\varphi_p))$ in Eq. (4). Note that Eq. (4) results from the competition between the torque exerted by the applied field on the magnetization vector inside the DW and in-plane forces resulting from the demagnetizing field and in-plane anisotropy. Let us describe the onset of DW anisotropic velocity. As far as h is smaller than h_{W1} [$h_{W1}=(1-\chi_4)$ for $\chi_4<1/4$ or $h_{W1}=(1/8\chi_4+\chi_4)$ for $\chi_4>1/4$] a solution of Eq. (4) in the steady regime ($\dot{\varphi}=0$) can be found for any orientation φ_p of the DW. The velocity is then linear with the field and isotropic. At $h=h_{W1}$ (velocity v_{W1}) the precessional regime is reached for four orientations of the DW, $\varphi_{p1}=-\pi/8+n\pi/2$, $n=(0,3)$, corresponding to the normal to the edges of the square domains. Hence, above h_{W1} the DW velocity becomes anisotropic, being smaller along the φ_{p1} directions. As h further increases, the range of orientations φ_p with a solution still in the steady regime (larger velocity) shrinks around four values $\varphi_{p2}=+\pi/8+n\pi/2$, $n=(0,3)$ corresponding to the diagonals of the square domains. At $h_{W2}=1+\chi_4$, the precessional regime is finally reached for those φ_{p2} values at a velocity $v_{W2}=v_W(1+\chi_4)$. Above h_{W2} the DW velocity remains anisotropic (see the insets of Fig. 2) but this anisotropy vanishes at large field ($h\gg 1$ and $h\gg\chi_4$), as shown by Eq. (6).

Figure 2 shows a comparison between the predicted and measured velocities in the directions $\varphi_p=-\pi/8$ (normal to the edge) and $\varphi_p=\pi/8$ (along the diagonal). As proposed in Ref. 18, the slopes of the low ($1<h<1.5$) and high drive ($h>12$) linear regimes were fitted with the predictions for the steady and the linear precessional regimes, respectively [see also Fig. 1(e)]. Δ and α are thus obtained self-consistently. For χ_4, we use the value deduced from FMR measurements (0.6). The discrepancy between the predicted and measured velocities at low drive ($h\approx 1$) is due to DW pinning. It prevents a precise comparison of the predicted h_1 value with experimental results since the width of the measured velocity distribution is larger than the difference between the calculated velocities $v(\varphi_p=\pi/8)$ and $v(\varphi_p=-\pi/8)$. Beyond the linear steady-state regime ($1.5<h<9$) the predicted average velocity is smaller than the measured one. This points to the limitations of the 1D model to describe DW motion. Indeed it does not take into account the temporal instabilities of DW motion (generation and propagation of horizontal Bloch lines) nor the spatial instabilities such as the wall-displacement waves.[19] This discrepancy may also suggest a modification of the dissipation mechanisms in this field range. In contrast, the predicted values for h_{W2} and v_{W2} coincide well with the end of the observed steady-state regime for $\varphi_p=\pi/8$. Note that h_{W2} lies below the field corresponding to the experimental maximum velocity, which is located well inside the precessional regime and should not be confused with a Walker peak. Moreover the upper boundary of the anisotropic regime ($h=5.5$–7.0) is also in good agreement with the predictions. Therefore, the field range for the existence of an anisotropic DW velocity is well accounted for by the model.

The domain growth is modeled using contour dynamics.[27] Pseudospectral techniques[28] are used to solve for the time evolution of the local tangent angle $\vartheta(s)$, from which the $[x(s),y(s)]$ coordinates of the interface are computed by ba-

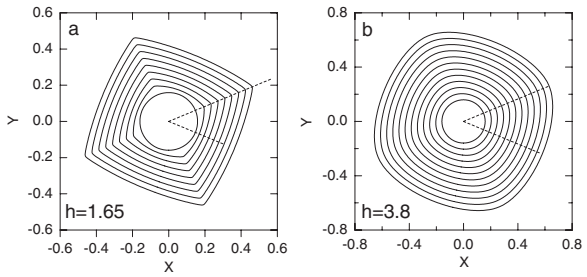

FIG. 3. Magnetic domain growth from contour dynamics at $h=1.65$ and at $h=3.8$. The coordinates of the DW are scaled with respect to the perimeter of the initial circular shape $L(0)$. Time is scaled with respect to $L(0)/v_W$. Domain shapes are shown from $t=0$ to $t=0.4$ by step 0.05 in (a) and from $t=0$ to $t=1.1$ by step 0.1 in (b). The directions of minimal and maximal displacements for the time interval, as calculated from Eqs. (3)–(6) are shown by dashed lines.

sic differential geometry. The normal velocity is obtained from Eq. (5) and (6). The dynamics of the domain shape is shown for $h>h_{W2}$ in Fig. 3(a) ($h=1.65$) and 3(b) ($h=3.8$). First the square domain shape is obtained [Fig. 3(a)], in excellent agreement with the experimental observations. As h increases the square shape evolves toward a rounded shape [Fig. 3(b)]. For still larger field strength, for example such that corresponds to Fig. 1(c), contour dynamics shows that the shape of domains remains close to circular as expected according to Eq. (5) and (6). The domain orientation is also very well reproduced. The mean velocities of vertices and edges are indicated by circles in Fig. 2. They are smaller and larger, respectively, than the maximal and minimal velocity obtained from Eq. (5) and (6), the difference vanishing with increasing field.

In conclusion, we have shown that magnetic anisotropy of tetragonal symmetry results in the growth of square shaped magnetic domains. Domain walls are found to be aligned at $\pi/8$ from the anisotropy easy axes, i.e., away from the directions that minimize the interface energy. The 1D model for DW motion, brought into play together with contour dynamics, captures the main features of the physics of anisotropic domain growth (domain shape and orientation, field range), although it underestimates the DW velocity. The existence of an angle between the anisotropy easy axis and the direction of maximum DW velocity in dynamical regimes ($\pi/2$ for π symmetry, $\pi/8$ for $\pi/2$ symmetry) is specific to ferromagnetic systems and is associated to the vectorial nature of the order parameter. Interestingly, the combination of in-plane biaxial and uniaxial anisotropy of similar importance that may occur in some range of temperature for ferromagnetic semiconductors should lead to the observation of complex domain shapes. The occurrence of anisotropic DW velocity should have important implications for the study of DW motion in micro- or nanoribbons for information storage and transport.

This work was in part supported by Région Ile de France (Contract No. C'Nano IF07-800/R).

[1] J. Deschamps, M. Georgelin, and A. Pocheau, Europhys. Lett. **76**, 291 (2006).
[2] S. Akamatsu, G. Faivre, and Thomas Ihle, Phys. Rev. E **51**, 4751 (1995).
[3] D. A. Kessler, J. Koplik, and M. Levine, Adv. Phys. **37**, 255 (1988).
[4] A. T. Dorsey and O. Martin, Phys. Rev. A **35**, 3989 (1987).
[5] H. Ellmer *et al.*, Surf. Sci. **476**, 95 (2001).
[6] J. B. Hannon, J. Tersoff, and R. M. Tromp, Science **295**, 299 (2002).
[7] A. Bodmer, U. Essmann, and H. Träuble, Phys. Status Solidi A **13**, 471 (1972).
[8] P. W. Shumate, J. Appl. Phys. **42**, 5770 (1971).
[9] A. P. Malozemoff and K. R. Papworth, J. Phys. D **8**, 1149 (1975).
[10] D. J. Breed, A. M. J. van der Heijden, H. Logmans, and A. B. Voermans, J. Appl. Phys. **49**, 939 (1978).
[11] D. J. Breed, P. Q. J. Nederpel, and W. de Geus, J. Appl. Phys. **54**, 6577 (1983).
[12] V. V. Randoshkin, Phys. Solid State **39**, 1260 (1997).
[13] P. Haibach, M. Huth, and H. Adrian, Phys. Rev. Lett. **84**, 1312 (2000).
[14] S. Bodea, W. Wulfhekel, and J. Kirschner, Phys. Rev. B **72**, 100403(R)(2005).
[15] N. L. Schryer and L. R. Walker, J. Appl. Phys. **45**, 5406 (1974).
[16] J. C. Slonczewski, J. Appl. Phys. **44**, 1759 (1973); **45**, 2705 (1974).
[17] P. J. Metaxas, J. P. Jamet, A. Mougin, M. Cormier, J. Ferré, V. Baltz, B. Rodmacq, B. Dieny, and R. L. Stamps, Phys. Rev. Lett. **99**, 217208 (2007).
[18] A. Dourlat, V. Jeudy, A. Lemaître, and C. Gourdon, Phys. Rev. B **78**, 161303(R) (2008).
[19] E. Schlömann, IEEE Trans. Magn. **10**, 11 (1974).
[20] C. H. Tsang, R. L. White, and R. M. White, J. Appl. Phys. **49**, 6052 (1978).
[21] E. Schlömann, J. Appl. Phys. **47**, 1142 (1976).
[22] T. Jungwirth, J. Sinova, J. Mašek, J. Kucera, and A. H. MacDonald, Rev. Mod. Phys. **78**, 809 (2006).
[23] A. Dourlat *et al.*, J. Appl. Phys. **102**, 023913 (2007).
[24] Kh. Khazen, H. J. von Bardeleben, M. Cubukcu, J. L. Cantin, V. Novak, K. Olejnik, M. Cukr, L. Thevenard, and A. Lemaitre, Phys. Rev. B **78**, 195210 (2008).
[25] C. Gourdon, A. Dourlat, V. Jeudy, K. Khazen, H. J. von Bardeleben, L. Thevenard, and A. Lemaitre, Phys. Rev. B **76**, 241301(R) (2007).
[26] L. Thevenard, L. Largeau, O. Mauguin, G. Patriarche, A. Lemaitre, N. Vernier, and J. J. Ferré, Phys. Rev. B **73**, 195331 (2006).
[27] T. Y. Hou, J. S. Lowengrub, and M. J. Shelley, J. Comput. Phys. **114**, 312 (1994).
[28] C. Canuto, M. Y. Hussaini, A. Quarteroni, and T. A. Zang, *Spectral Methods in Fluid Dynamics* (Springer-Verlag, Berlin, 1988).